Chemistry and Physics of Lipids 218 (2019) 178–186

Contents lists available at ScienceDirect

Chemistry and Physics of Lipids

journal homepage: www.elsevier.com/locate/chemphyslip

Mechanical properties of bilayers containing sperm sphingomyelins and ceramides with very long-chain polyunsaturated fatty acids

H. Ahumada-Gutierrez[a,c], D.A. Peñalva[d], R.D. Enriz[b], S.S. Antollini[d], J.J. López Cascales[a,*]

[a] Departamento de Ingeniería Química y Ambiental, Universidad Politécnica de Cartagena, Grupo de Bioinformática y Macromoléculas (BIOMAC), Aulario II, Campus de Alfonso XIII, 30203 Cartagena, Murcia, Spain
[b] Universidad Nacional de San Luis, Facultad de Química, Bioquímica y Farmacia, IMIBIO-CONICET, Chacabuco 917, 5700 San Luis, Argentina
[c] Universidad del Bio-Bio, Departamento de Ciencias BásicasFacultad de Ciencias, Av. Andrés Bello S/N, Casilla 447, Chillan, Chile
[d] Instituto de Investigaciones Bioquímicas de Bahía Blanca, Departamento de Biología, Bioquímica y Farmacia, Universidad Nacional del Sur-CONICET, Bahía Blanca, Argentina

ARTICLE INFO

Keywords:
2-Hydroxy ceramides
Bending rigidity
Bilayer compressibility
Gaussian curvature modulus
Sphingomyelins

ABSTRACT

Sphingomyelins (SM) and ceramides (Cer) with very long chain polyunsaturated fatty acids (V) are important components of spermatozoa membranes. In this study, the mechanical properties of bilayers of SM and Cer with nonhydroxy (n-V) and 2-hydroxy (h-V) fatty acid (30:5) were studied by molecular dynamics simulation at different temperatures and in the presence and the absence of salt. From our results, it was evidenced how n-V SM and h-V SM bilayers showed similar behavior. When n-V Cer was added to a h-V SM bilayer, the Gaussian curvature modulus and E_{curve} of binary bilayers decreased. This variation in the mechanical properties of the bilayer can be associated with an incipient step during the fecundation process.

1. Introduction

Sphingomyelins (SM) and ceramides (Cer) are known to have sphingosine as their long-chain base (an amine diol of 18 carbon atoms, hydroxyl groups at carbons 1 and 3, and a trans double bond between its carbons 4 and 5), whose nitrogen atom at C-2 is amide-bound to a long-chain fatty acid. The hydroxyl groups on carbons 1 and 2 of sphingosine are free in Cer, but in SM the former is ester-bound to a phosphocholine polar head group. The most abundant acyl chains of SM in mammalian tissues are 16 to 24 carbon length fully saturated (16:0-24:0) or monounsaturated (16:1-24:1) fatty acids (Barenholz and Thompson, 1980; Ramstedt and Slotte, 2002). A noticeable exception are the SM of the testis and spermatozoa of various mammals including human (Poulos et al., 1986, 1987), in which they contain an infrequent series of very long chain (C24 to C34) polyunsaturated fatty acids (VLCPUFA). In some mammals including the common laboratory rats, an important percentage of these fatty acids contain a 2-hydroxyl group, which add another peculiarity to these sphingomyelins (Robinson et al., 1992).

In addition to SM, these atypical fatty acids are also important components of ceramides in rat spermatogenic cells and spermatozoa (Furland et al., 2007; Oresti et al., 2010; Zanetti et al., 2010). The most abundant VLCPUFA are tetraenoic and pentaenoic fatty acids of the n-6 series, of which 28:4n-6, 30:5n-6, and 32:5n-6 are the major non-hydroxy-VLCPUFA (n-V) and the corresponding 2-hydroxylated versions are the major 2-hydroxy-VLCPUFA (h-V). In the rat testis, the ratio between h-V and n-V in SM and Cer increases with post-pubertal maturation (Zanetti et al., 2010) and in the adult testis with germ cell differentiation (Oresti et al., 2010), as n-V SM and n-V Cer species predominate in spermatocytes and the corresponding h-V species in spermatids and spermatozoa. In gametes, the n-V SM and h-V SM, which are located specifically on the heads (Oresti et al., 2011), are converted into the corresponding ceramides (n-V Cer, h-V Cer), by the action of an endogenous sperm sphingomyelinase, after completion of the acrosomal reaction (Oresti et al., 2015), a reaction that must occur in the membrane of a spermatozoon before it becomes competent to fertilize an oocyte.

Considering their peculiar structure, their unique and specific cellular location, and their involvement in a chemical reaction with those important biological implications, the biochemical and biophysical study of these species is of great interest (Slotte and Ramstedt, 2007; Piotto et al., 2014). Regarding their biophysical properties, the number of studies is quite limited in comparison with the intensive attention that some species of SM and Cer have received during the last decades. Previous works on bilayers (Peñalva et al., 2013) and monolayers (Peñalva et al., 2014a, 2014b) of these species showed that the

* Correspondence author.
E-mail address: javier.lopez@upct.es (J.J.L. Cascales).

https://doi.org/10.1016/j.chemphyslip.2018.12.008
Received 11 July 2018; Received in revised form 17 December 2018; Accepted 19 December 2018
Available online 03 January 2019
0009-3084/

behavior of SM with VLCPUFA differs in many aspects from the ones measured in typical SM and Cer species (Veiga et al., 1999; Jimenez-Rojo et al., 2014). Thus, for example, in unilamellar vesicles containing phosphatidylcholine (PC), SM and cholesterol, it has been observed that these SM do not present a tendency to form discrete domains in the same conditions as 16:0 SM (Peñalva et al., 2013). In monolayers, n-V Cer and h-V Cer showed larger molecular areas than 16:0 Cer or 24:1 Cer, where the presence of the 2-hydroxyl group induced an increase in the molecular packing and dipole momentum (Peñalva et al., 2014a).

As far as we know, experimental information concerning structural and mechanical properties of bilayers formed by SM and Cer with VLCPUFA has not been reported. Molecular dynamics (MD) simulation is a powerful technique to gain insight into the behavior of these molecules when they are assembled in a lipid bilayer, that provides relevant and reliable information about dynamic and steady properties of these molecular bilayers. Many properties related with the structure and dynamic properties of SM bilayers containing saturated fatty acids like 18:0 SM or 16:0 SM have been studied by MD simulation (Chiu et al., 2003; Hyvonen and Kovanen, 2003; Mombelli et al., 2003; Niemela et al., 2004; Pandit and Scott, 2006; Guo et al., 2013; Dutagaci et al., 2014) and their results have been ratified with experimental data (Maulik et al., 1991; Mombelli et al., 2003).

In this context, MD simulations have been addressed to understand the role played by SM in the formation of lipid rafts in the cell membrane, and the role of SM as precursor of bioactive molecules, in particular of Cer. Thus, a great number of studies on Cer have been focused on the role played by Cer as a signaling molecule in several biological processes. Moreover, recent studies showed that these species are excluded from raft-like structures that can be isolated from the plasma membrane of spermatogenic cells (Valtierra et al., 2017).

Thus, the aim of this work is to investigate the mechanical properties of SM bilayers with VLCPUFA, and how Cer perturbs the properties (at a molecular level) of SM bilayer when they are present. MD simulations were performed with atomic detail of SM and Cer, having 2-hydroxy 30:5 n-6 (h-V SM and h-V Cer) and nonhydroxy 30:5 n-6 (n-V SM and n-V Cer) as the amide-bound fatty acids. Beyond other questions, this work tries to answer how the presence of the 2-hydroxyl group in the fatty acyl chain affects the bilayer properties. Furthermore, mechanical properties as the compressibility modulus, bending modulus and Gaussian curvature modulus are estimated for the first time for these SM bilayers in the presence and the absence of Cer. Taking into account that n-V Cer and h-V Cer accumulate at the expense of the corresponding sphingomyelins on the rat sperm head membrane during the acrosomal reaction (Oresti et al., 2015), different Cer:SM molar ratios have been investigated in order to determine the impact that such transformation has on the curvature and Gaussian curvature moduli of the original SM bilayer.

2. Models and methods

Fig. 1 shows the two species of SM and Cer studied in this work. Thus, we will refer to them as h-V SM and h-V Cer when the fatty acid amide bound to sphingosine is 2-hydroxy 30:5 n-6, or n-V SM and n-V Cer when the fatty acid is nonhydroxy 30:5 n-6. The molecular weights of h-V SM and h-V Cer are 904.6 g/mol and 739.7 g/mol, respectively, and 888.6 g/mol and 723.7 g/mol for n-V SM and n-V Cer, respectively (Valtierra et al., 2017). Table 1 shows the atomic charge distributions of x-V SM and x-V Cer employed in our simulations, that were calculated using the semi-empirical Complete Neglect of Differential Overlap (CNDO) method (Pople and Segal, 1966) included in the Hyperchem package (HyperChem, 1992). GROMACS 4.5.3 (Berendsen et al., 1995; Lindahl et al., 2001) was used to carry out the MD simulations, and 4 fs was the integrator time step in all the simulations. All the bilayers of this work were constituted by 128 molecules of SM or Cer (or a mixture of them, maintaining constant the 128 molecules in total) and 4616 water molecules of the SPC water model (Berendsen et al., 1981). Fig. 3

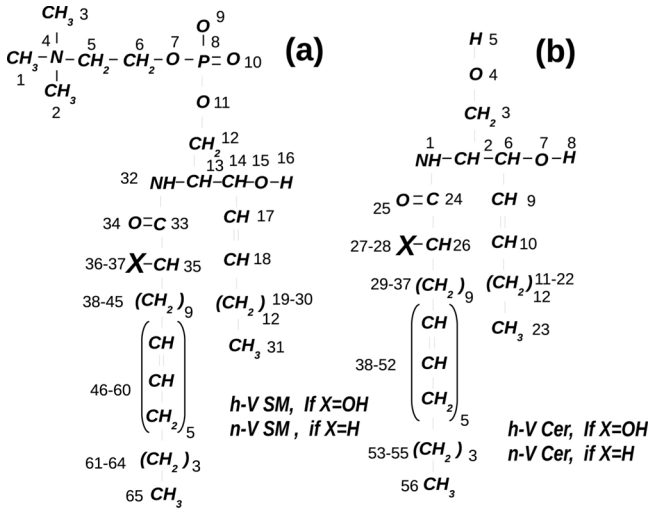

Fig. 1. Scheme of the sphingomyelin (a) and ceramide (b) species with very long-chain PUFA 30:5 n-6 examined in this study. The letter X, bound to the second carbon atom of the fatty acid, in this case 30:5 n-6, is a hydroxyl group -OH in the SM and Cer with 2-hydroxy 30:5 (h-V SM and h-V Cer, respectively) or -H in the SM or Cer with nonhydroxy 30:5 (n-V SM or n-V Cer, respectively).

shows snapshots of the four bilayers studied in this work, after equilibration time. In our simulation, we consider that both h-V SM and h-V Cer correspond to pure + chiral species.

Particle Mesh Ewald method (Darden et al., 1993; Essmann et al., 1995) was used for calculating the electrostatic contribution. Coordinates and velocities were recorded every 5 ps of simulation time. Chemical bonds were constrained using the LINCS algorithm (Hess et al., 1997). Simulations were coupled to an external temperature and pressure bath, using the Berendsen algorithm (Berendsen et al., 1984), with temperature and pressure coupling constants of 0.1 and 1 ps, respectively. The length of all the simulated trajectories was of 400 ns, of which the first 100 ns were discarded from analysis as equilibration time of the systems, as it is seen in Fig. 2. Error bars of all the properties studied in this work were estimated from sub-trajectories of 50 ns each, over the last 300ns of the simulated trajectories.

Bilayers were simulated at 300 K, 310 K and 330 K. Furthermore, at 310 K, the SM bilayers were also simulated in the presence of 0.5 M NaCl to determine the effect of the ionic strength on their mechanical properties.

GROMOS force field (van Gunsteren and Berendsen, 1987) was used as base of all our simulations. The LJ parameters, bond angles, dihedral interactions and force constants used in these simulations for DM and Cer were the same than the proposed by Egberts et al. (Egberts et al., 1994) and that has been tested in previous simulations of lipid bilayers (López Cascales et al., 1998, 1997, 2006; Porasso et al., 2009; Giner Casares et al., 2010; López Cascales et al., 2012; Bahamonde-Padilla et al., 2013). The improper dihedral corresponding to $-CH_2-CH_2-CH_2-CH_2-$, we used the Ryckaert-Bellemans potential (Ryckaert and Bellemans, 1978).

3. Results and discussion

3.1. Mechanical properties of pure bilayers.

3.1.1. Local pressure profile, Π(z)

The structure and function of protein membranes are sensitive to their membrane microenvironement, including the membrane thickness, its fluidity and, especially, its lateral pressure profile (der Laan van den Brink-van et al., 2004). This local pressure in bilayers increased because lipid bilayers are inhomogeneous soft systems in which the hydrophilic head groups are squeezed together to prevent the exposure

Table 1
Atomic charge distribution of SM and Cer studied in this work according to the atom numeration of Fig. 1. The data were calculated using the semi-empirical CNDO method.

Atom in group	Label	h-V SM	Label	n-V SM	Label	h-V Cer	Label	n-V Cer
Aliphatic methyl group	1-3	0.175	1-3	0.175	–		–	–
Choline nitrogen	4	0.086	4	0.086	–		–	–
Aliphatic methylen group	5	0.161	5	0.161	–		–	–
Aliphatic methylen group	6	0.074	6	0.074	–		–	–
Oxygen in ester bond	7	−0.373	7	−0.373	–		–	
Phosphorous	8	0.676	8	0.676	–		–	
Phosphate oxygen	9	−0.385	9	−0.385	–		–	
Phosphate oxygen	10	−0.385	10	−0.385	–		–	
Hydrogen in hydroxyl group	–	–	–	–	5	0.282	5	0.380
Oxygen in hydroxyl group	–	–	–	–	4	–	4	–
Oxygen in ester bond	11	−0.379		−0.379	–		–	–
Aliphatic methylene ($-CH_2-$)	12	0.089	12	0.089	3	0.200	3	0.200
Aliphatic methylene ($-CH-$)	13	0.079	13	0.079	2	0.180	2	0.180
Aliphatic methylidyne ($-CH-$)	14	0.119	14	0.119	6	0.276	6	0.280
Hydroxyl oxygen	15	−0.347	15	−0.347	7	0.552	7	0.600
Hydroxyl hydrogen	16	0.141	16	0.141	8	0.284	8	0.240
Alkenic methylidyne (-C=)	17	0.010	17	0.010	9	0.064	9	0.060
Alkenic methylidyne (=C-)	18	−0.091	18	−0.091	10	−0.066	10	0.020
Aliphatic methylenes ($-CH_2-$)	19-30	0.000	19-30	0.000	11-22	0.000	11-22	0.000
Aliphatic methyl group ($-CH_3$)	31	0.000	31	0.000	23	0.000	23	0.000
Amide nitrogen	32	−0.090	32	−0.074	1	−0.140	1	−0.200
Carbonyl carbon	33	0.437	33	0.416	24	0.600	24	0.740
Carbonyl oxygen	34	−0.334	34	−0.379	25	−0.560	25	−0.840
Methylidene or Methylene	35	0.087	35	0.010	26	0.188	26	0.100
Hydroxyl oxygen	36	−0.254	–	–	27	−0.516	–	–
Hydroxyl hydrogen	37	0.154	–	–	28	0.280	–	–
Aliphatic methylenes ($-CH_2-$)	38	0.000	36	0.036	29	0.000	27	0.000
Aliphatic methylenes ($-CH_2-$)	39-45	0.000	37-43	0.000	30-37	0.000	28-35	0.000
Aliphatic methylidynes (-C=)	46-60	0.000	44-58	0.000	38-52	0.000	36-50	0.000
Aliphatic methylenes ($-CH_2-$)	61-64	0.000	59-62	0.000	53-55	0.000	51-53	0.000
Aliphatic methyl group	65	0.000	63	0.000	56	0.000	54	0.000

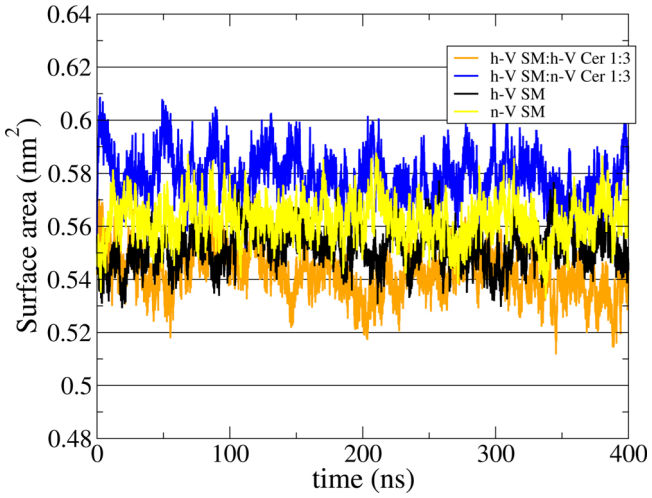

Fig. 2. Running surface area per molecule of both SM bilayers and two of the binary bilayers studied in this work.

of the hydrophobic tails to the aqueous solution. For lipid bilayer in equilibrium, the net tension is zero, because the superficial tension at the level of the head groups is balanced by the expansion of their lipid tails, which tend to maximize their entropy trying to occupy the whole volume inside the membrane. As far as we know, no information is available about the lateral pressure of bilayers formed by lipids with VLCPUFA, as the studied in this work. In fact, direct and unambiguous measurements of lateral pressures in lipid bilayers are not experimentally available, mainly because the forces that rule the shrinking and expansion in bilayers are so tiny (such as it corresponds to soft matter) that they are not easy to measure except in very limited exceptions (Templer et al., 1998).

In MD simulations, pressure can be determined from the pressure tensor **P** expressed as follows,

$$P = \left(\sum_i m_i v_i \otimes \ v_i - \frac{1}{V} \sum_{i<j} F_{ij} \otimes \ r_{ij} \right) \quad (1)$$

where the first term corresponds to the kinetic energy of the system, E_k, and the second one is related with the molecular virial of the system, Ξ; m_i and v_i corresponds to the mass and velocity of each particle of the system, and finally, r_{ij} and F_{ij} correspond to the distance and force between two particles, $i-j$, respectively. The pairwise interactions include non-bonded forces (electrostatic and van der Waals interactions) and covalent interactions between bonded atoms. Because pressure tensor P is calculated in equilibrium, the terms of this tensor outside the diagonal can be ignored.

Since the electrostatic contribution in our simulations is calculated using a long range electrostatic interaction by the Particle Mesh Ewald method (Darden et al., 1993; Essmann et al., 1995), and because it can not be decomposed in F_{ij} terms, the contribution of the electrostatic interactions must be recalculated using a cut-off method based on the Lindahl and Edholm approximation that has been described elsewhere (Lindahl and Edholm, 2000). In our case, we re-used the trajectories previously generated with the Particle Mesh Ewald method, as it was described in Section 2, but in this case, we employed a value of rlist of 2.0nm for the short cut-off, and a value of of 2.2nm for the long cut-off corresponding to coulomb (rcoulmb) and van der Waals (rvdw) interactions.

Fig. 4 shows the pressure profiles obtained for the SM and Cer bilayers with VLCPUFA, at 310 K. At the left and right extremes of the four profiles, the net lateral pressure was zero, as expected for bulk water in equilibrium. In equilibrium, to guarantee mechanical stability of the bilayers, the integral lateral pressure profiles across the membrane should be zero, as it is seen in Fig. 4 where the continuous integral for the four bilayers studied is zero. This result supports the idea

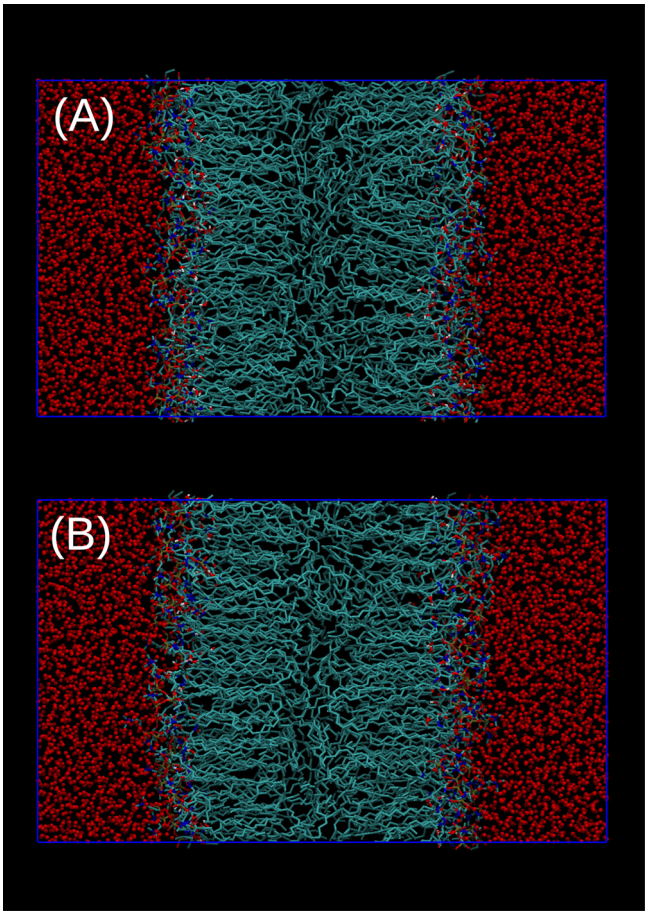

Fig. 3. Snapshots of the four bilayers studied in this work, after 100 ns of simulation time. (A) h-V SM and (B) n-V SM. Water molecules are shown as red beads.

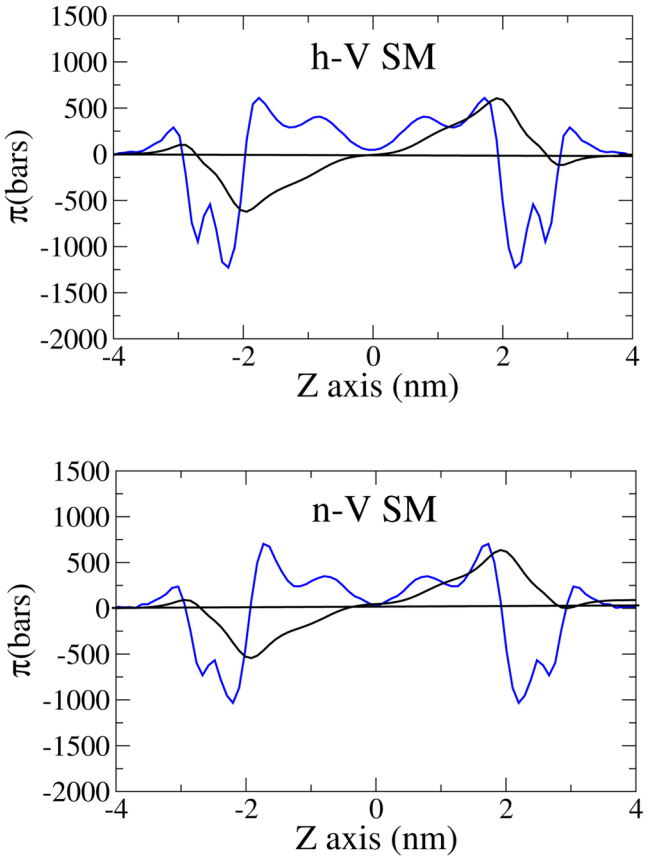

Fig. 4. Lateral pressure profile π(z) of SM bilayers at 310 K (blue line). Line in black represents the cumulative integral of π(z) The origin of z axis was placed at the middle of the bilayer.

that the bilayers studied are in equilibrium.

For the two sphingomyelins, upon entering into the membrane at the head group region, there was a positive value for the lateral pressures, with values around 250 bar. This result reflects that the bilayer interfacial area presents a tendency to expand, due to repulsive interactions between neighboring SM head groups (due to steric, electrostatic, and hydration forces). At the polar/apolar interfaces, the profiles showed deep troughs in the lateral pressure with values around -1200 bar. This negative value is due to the interfacial tension that tries to shrink the bilayer to minimize the exposure of the hydrocarbon tails to the aqueous environment. In the bilayer interior, the pressure profile displayed positive values again, with values of 600 bar and 800 bar for h-V SM and n-V SM, respectively. These positive values are due to the fact that the chain packing is relatively tight in this area, the corresponding entropy loss causes significant repulsive forces between neighbouring tails, which explain these positive values. Penetrating into the bilayer, two pressure minima were observed, with an interposed maximum that may be ascribed to the part of the molecules where the double bonds are located. This supports our view that there is no significant tail interdigitation between the ultra-long fatty acyl chains of SM molecules located in each leaflet.

3.1.2. Compressibility and bending modulus

A lipid bilayer is a soft material that can be characterized by its elastic modulus. As bilayers are two-dimensional structures, their availability to be compressed (or stretched) laterally is proportional to their isothermal compressibility modulus, K_A. Thus, K_A gives a measure of the cohesion strength between the lipid molecules in the (x, y) plane of the orthogonal space, with the z axis being perpendicular to the bilayer plane. From simulation, K_A is calculated as follows (Rawicz et al., 2000):

$$K_A = \frac{k_B \mathrm{TA}}{\sigma^2(A)} \tag{2}$$

where A and $\sigma^2(A)$ correspond to the mean and mean-squared fluctuation of the surface area per molecule, respectively; k_B is the Boltzman constant, and T, the temperature in Kelvin degrees. Table 2 shows the different surface areas per molecule studied in this work.

Membranes resist bending perturbations because the alteration of their curvature modify both the head group spacing and the entropy of the hydrophobic chains. The flexibility of a lipid bilayer may be

Table 2
Surface area per molecule and bilayer thickness. The bilayer thickness was calculated from the amide nitrogen distributions of both leaflets. Values in parenthesis correspond to values previous reported in the bibliography.

Bilayer	Area/Å^2	d_{HH}/(Å)
	300 K	
h-V SM	53.9 ± 0.6 (53-55 Chiu et al., 2003; Maulik et al., 1991)	41.7 ± 0.6
n-V SM	54.3 ± 0.8	43.5 ± 0.3
	310 K	
h-V SM	55.6 ± 0.7	42.3 ± 0.2
n-V SM	55.8 ± 0.7	41.3 ± 0.9
	330 K	
h-V SM	55.8 ± 0.7 (52-56 Niemela et al., 2006)	41.4 ± 0.5
n-V SM	59.0 ± 0.8	40.2 ± 0.2
	310 K, 0.5 M NaCl	
h-V SM	55.3 ± 0.7	41.3 ± 0.7
n-V SM	56.0 ± 0.8	40.2 ± 0.6

characterized by the bending modulus k^b. Thus, low k^b values mean high membrane elasticity. Lipids with high degree of unsaturation produce very flexible membranes. For example, in a series of bilayers of phosphatidylcholines (PC) having 18 carbon atoms in both acyl chains, the species with two PUFA (di-18:3 PC, di-18:2 PC) are considerably more flexible (with k^b values of $0.4 \times 10^{-20} J$) than species having fatty acids with one or two double bonds, like 18:0-18:1 or di-18:1 PC (SOPC, DOPC), with average values of k^b around $0.9 \times 10^{-20} J$ (Rawicz et al., 2000).

From MD simulation, k^b of a lipid bilayer can be calculated using different theoretical and simulation approaches (Goetz et al., 1999; Watson et al., 2013; Levine et al., 2014; Venable et al., 2015; Doktorova et al., 2017) on the basis of the shape fluctuation in the bilayer membrane obtained from the spectrum analysis obtained from a Fourier analysis. A simple way of estimating k^b is based on the approximation to the Polymer Brush Model proposed by Rawicz et al. (2000), where k^b can be calculated as follows:

$$k^b = \frac{K_A \xi^2}{24} \tag{3}$$

being ξ the effective thickness of the lipid bilayer, with $\xi = d_{HH} - 1$ and d_{HH}, the bilayer thickness in nm (Rawicz et al., 2000), that is calculated as it was described above. Table 2 shows the values of thickness of SM bilayers studied in this work.

Fig. 5 shows the compressibility modulus, K_A, obtained for the SM bilayers at three different temperatures. Its highest value was of 372 mN/m for the h-V SM bilayer at 300 K and the lowest value was of 258 mN/m for n-V SM at 300 K. These values are of the same order of magnitude than the reported by Rawicz et al. (2000) for different phosphatidylcholine bilayers, with values that range from 230-265 mN/m. The lower values recorded in our study are associated to the much less cohesive nature of the present SM bilayers than those of 18:0 SM studied by Chiu et al. (2003).

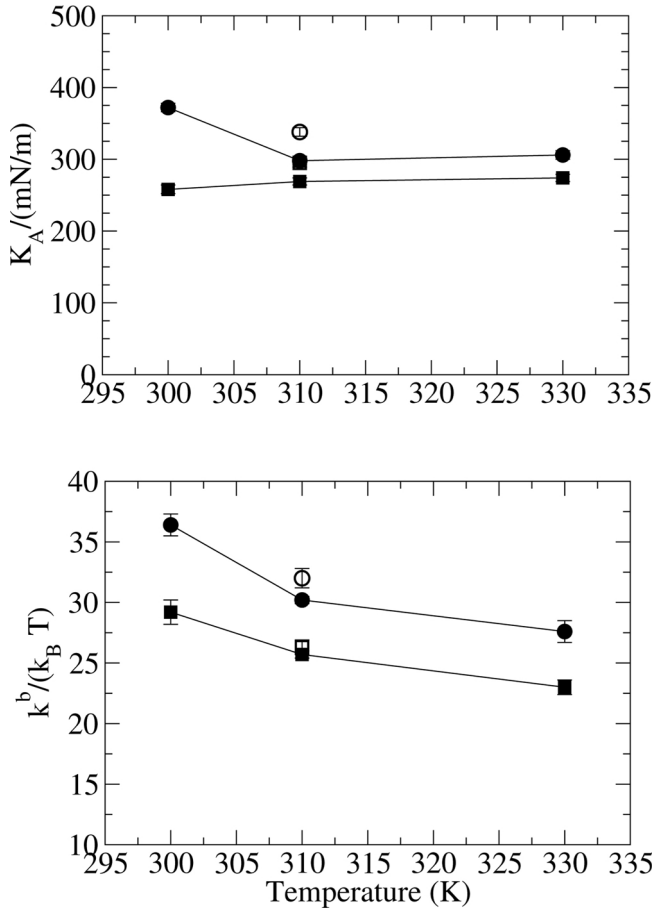

Fig. 5. Compressibility (K_A) and bending (k^b) modulus of the two sphingomyelins studied in this work at different temperatures. h-V SM (filled circle), n-V SM (filled square), h-V SM 0.5M NaCl (open circle), and n-V AM 0.5M NaCl (open square).

K_A of 468 and 426 mN/m were measured in bilayers of DPPC and DPPS, respectively (López Cascales et al., 2012), from MD simulation at 350 K (77 °C). These values are of the same order of magnitude than the estimated from our simulations in SM bilayers. As it was determined in vesicles by micropipette aspiration experiments (Rawicz et al., 2000), at 294 K, the highest K_A value of a serial of unsaturated PC was 244 mN/m for di-22:1-PC and also for di-18:3-PC. Our simulation results are also consistent with the value of K_A of 254 mN/m determined for di-18:1 PC (DOPC) via X-ray measurements at 303 K (Pan et al., 2008). Thus, K_A modulus of our SM presented intermediate values between those of DPPC and those of unsaturated PCs. At 288 K, the value of K_A increased from 193 mN/m to 333 mN/m for bilayers of 18:0-18:1 PC (SOPC) with the addition of 33 % cholesterol (Needham and Nunn, 1990), these results being also in good agreement with our simulation results. In the range of the temperatures studied, K_A was always higher for h-V SM than for n-V SM bilayers, indicating higher cohesive strengths between h-V SM molecules than in n-V SM bilayers, see Fig. 5. This difference may be attributed to the extra hydroxyl group present in the fatty acid of h-V SM. Interestingly, the difference in K_A between these SM species was the largest at low temperatures (300 K), where the interactions between neighboring molecules were much higher, as a consequence of the lower thermal agitation.

In Langmuir monolayers, the compressibility of h-V SM and n-V SM at room temperature and 30 mN/m of lateral surface pressure (represented by the Cs-1 modulus) presented values of 86 and 84 mN/m, respectively (Peñalva et al., 2014a).

One of the few studies of variation of the SM compressibility with temperature of SM with 12 to 26 carbons was carried out in monolayers at a constant pressure of 30 mN/m in a range from 283 to 303 K (Li et al., 2000). In their fluid phase, SM were less compressible than PC species with similar chain structures. In general, the Cs-1 modulus of the SM monolayers increased with the number of carbons and decreased with the presence of one double bond. Although in these cases two-dimensional phase transitions (from a liquid-expanded to a liquid-condensed nature) were observed at many of the temperatures studied, the compressibility decreased with an increase of temperature, in good agreement with our simulation results for h-V SM (Fig. 5). On the contrary, K_A increased slightly with temperature for n-V SM bilayers, Fig. 5.

Regarding k^b (bending modulus) of SM bilayers, they ranged from 36 k_BT (for h-V SM at 300 K) to 23 k_BT (for n-V SM at 330 K), Fig. 5. For each of the temperatures studied, k^b was always higher in the h-V SM bilayer than in the corresponding n-V SM bilayer. Thus, the hydrogen bonds between neighbour 2-hydroxyl groups of the fatty acid contributed to the cohesion forces in the interfacial region, making the bilayers of h-V SM more rigid than those formed by n-V SM.

The k^b values estimated from our simulations are in the same order of magnitude than the previous simulation data of $42.1 \times 10^{-20} J$ (94 k_BT) for bilayers of 18:0 SM at 323 K, and the value of 4×10^{-20} J (9 k_BT) obtained for DPPC bilayers (Chiu et al., 2003), and the experimental data of 5×10^{-20} J (11k_BT) of DPPC bilayers at 323 K. Furthermore, our results are also in perfect agreement with the values of 16.4 k_BT and 34.8 k_BT reported for DPPC and DPPS, respectively (López Cascales et al., 2012).

Using single-wall vesicles manipulated by micropipette aspiration at room temperatures, k^b values cannot be experimentally obtained for species of SM or PC with long-chain saturated fatty acids (due to their high T_m and the bilayer vesicle instability below their T_m), but they were obtained at 294 K for a series of PC species whose fatty acids differed in the degree of unsaturation in one or in both of their acyl chains (Rawicz et al., 2000). Thus, their k^b modulus was also

determined on the basis of the Polymer Brush Model proposed by Rawicz et al. (2000) where k^b varied from 22.2 k_BT for 18:0-18:1 PC, to 20.9 k_BT for di 18:1-PC, and from this value to 29.6 k_BT for di 22:1 PC. These results illustrate the fact that k^b tends to decrease with the number of double bonds in one of the acyl chains and to increase with the number of carbon atoms in the lipid molecule. However, Rawicz et al. (2000) also showed that the presence of polyunsaturation in one or both chains introduced an exception. When passing from 18:0/18:1-PC to 18:0-18:2 PC bilayers, k^b values were reduced by a factor around 2, passing from 22.2 to 11.3 k_BT. However, an increase in the number of double bonds (maintaining the number of carbons e.g., 18:3-18:3 PC) kept the k^b values similar to the latter. Our results for h-V SM and n-V SM were of 36 k_BT and 29 k_BT, respectively, at 300 K, suggesting that the increase in the number of carbons is compensated by the decreasing effect associated with its poly-unsaturation, making the present bilayers less elastic than bilayers with unsaturated species.

Fig. 5 shows how, for h-V SM and n-V SM, k^b decreased with the increase of temperature. From X-ray, Pan et al. (2008) showed for unilamellar vesicles of DOPC how k^b followed a similar tendency to the obtained from our simulations, with values of 21.4, 18.2 and 16.3 k_BT for 15, 30 and 45 °C, respectively.

Fig. 5 shows how in SM bilayers K_A and k^b remains almost invariable in the presence of salt. This behavior is consistent with the idea that both SM bilayers are in the same fluid phase at this temperature (Peñalva et al., 2013). In addition, the effect of the presence of salts on the T_m is weaker for bilayers containing amphiphilic lipids, as it has been shown in PC bilayers, while T_m decreases more noticeably with salt in bilayers with acidic heads (Trauble and Haynes, 1971).

In previous studies carried out in our group (López Cascales et al., 2012), it has been measured as the presence of salt (0.5 M NaCl) affects in an opposite manner to DPPC and DPPS bilayers, where a diminishing for K_A and k^b of -13% and -3% and an increase of + 18% and +14% were estimated for DPPC and DPPS, respectively.

3.1.3. Spontaneous mean curvature, C_0

Lipid composition affects the local shape of membranes. Thus, lipids with cylindrical shape, like phosphatidylcholine or sphingomyelins, preferentially form flat bilayer structures. Lipids with an inverted conical shape as lysophospholipids, polyphosphoinositides and glycosphingolipids, form structures with positive curvature, and lipids with a small hydrophilic part in comparison with their hydrophobic cross section, such as PE, cardiolipin, diacylglycerol, and also ceramides, have conical shapes and form structures with negative curvature. Compared with other SM, the unusual fatty acids of our SM suggest that their spontaneous shape may not necessarily fit to the classical cylindrical shape. For the same reason, Cer molecules with VLCPUFA may be expected to exaggerate the conical shape that ceramides adopt.

From the calculation of the first and second moment defined as,

$$P_1 = \int_0^\infty z\Pi(z)\mathrm{d}z \tag{4}$$

$$P_2 = \int_0^\infty z^2\Pi(z)\mathrm{d}z \tag{5}$$

the spontaneous mean curvature of a lipid monolayer, C_0^m, can be calculated as $P_1 = k^m.\ C_0^m$ (Shearman et al., 2006), being k^m the leaflet bending modulus (that can be approximated to $k^b/2$), P_1 the first moment defined in equation (4) and $\pi(z)$ is the lateral pressure profile across the lipid bilayer,.

In surfactant monolayers, the spontaneous curvature C_0 describes the tendency of a molecular film to bend towards bulk water ($C_0 < 0$) or towards oil ($C_0 > 0$). By convention, the curvature is defined as convex for positive curvatures (normal oil-in-water) and concave for negative curvatures (inverted water-in-oil). The spontaneous curvature of a bilayer results from the competition between the packing areas of the polar heads and their hydrocarbon tails.

Table 3 shows as all the x-V SM present negative values of C_0 in line with their tendency of bending toward the water region.

Table 3
First moment P_1, spontaneous mean curvature C_0, Gauss Modulus K_G^b and Curvature Energy E_{curve} for the two SM bilayers studied in this work.

Bilayer	T (K)	$P_1/(k_BT.\ nm)$	C_0/nm	$K_G^b/(k_BT)$	$E_{curve}/(k_BT)$
h-V SM	300	−13.2 ± 0.8	−0.66 ± 0.18	90 ± 5	2147 ± 169
	310	−16.0 ± 0.6	−1.06 ± 0.05	87 ± 7	1858 ± 220
	330	−11.4 ± 1.2	−0.83 ± 0.04	76 ± 4	1668 ± 144
	310*	−10.4 ± 0.8	−0.65 ± 0.7	96 ± 3	2015 ± 300
n-V SM	300	−13.7 ± 0.3	−0.92 ± 0.08	96 ± 8	1931 ± 170
	310	−12.0 ± 0.7	−0.95 ± 0.12	84 ± 10	1697 ± 250
	330	−10.8 ± 0.6	−0.94 ± 0.07	70. ± 4	1458 ± 43
	310*	−11.9 ± 0.2	−0.913 ± 0.14	99 ± 13	1900 ± 280

* refers to the presence of 0.5 M NaCl.

3.1.4. Gaussian curvature moduli

K_G^b modulus is known as the Gaussian curvature modulus, which measures the energy cost of producing saddle-splay conformations in the membrane. The Gaussian curvature modulus is very difficult to measure experimentally, being available only in monolayers under special conditions and in a very reduced number of bilayers (Hu et al., 2013). In the present study, these values were estimated using the local pressure profile $\pi(z)$ measured in the previous section of this work (Safran, 1999), following a similar methodology to that proposed by Orsi et al. (2008) for DMPC bilayers. Thus, the Gaussian curvature modulus K_G^b of a lipid bilayer can be estimated as follows (Helfrich and Rennschub, 1990),

$$K_G^b = 2(K_G^m - 2k^m C_0^m \xi) \tag{6}$$

where K_G^m corresponds to the Gaussian curvature modulus, k^m to the bending modulus, and C_m^0 to the spontaneous monolayer curvature (the curvature of each leaflet of the bilayer in equilibrium), while ξ is the pivotal surface of the bilayer (the surface at which there is no change in the molecular cross-sectional area upon bending), where m refers to both monolayers (or leaflets) that form the lipid bilayer. Hence, K_G^m can be calculated as follows,

$$K_G^m = -\int_0^\infty (z-\xi)^2\pi(z)\mathrm{d}z = 2\xi P_1 - P_2 \tag{7}$$

being z = 0 the middle of the lipid bilayer, and P_1 and P_2, the first and second moment defined in equation (4) and (5), respectively.

K_G^b is positive in films that prefer isotropic shapes such as spheres or planes (Shearman et al., 2006). Table 3 depicts the Gaussian modulus, K_G^b, for all the bilayers studied in this work at different temperatures. We see in Table 3 how K_G^b modulus was positive in all the cases, showing the tendency of all the species to form bilayers.

Furthermore, Table 3 shows how K_G^b increases with the presence of salt.

3.1.5. Energy of curvature, E_{curve}

Claessens et al. (2004) proposed that bilayer stability is a combination of its bilayer bending modulus, k^b, and its Gaussian curvature modulus, K_G^b. Thus, bilayers mechanically stable are only found if the energy associated with the bending of a bilayer into a spherical shape is positive (Claessens et al., 2004). Therefore, in a first approximation and considering that the system goes from a planar to a spherical geometry, the energy needed to curve a flat bilayer into a closed vesicle, E_{curve}, is obtained from k^b and K_G^b, as follows: $E_{\mathrm{curve}} = 4\pi(2k^b + K_G^b)$ (Claessens et al., 2004). Table 3 shows the energy, E_{curve}, for all the range of temperatures and bilayers studied in this work.

Table 3 shows that all the values of E_{curve} were positive in bilayers of SMs, seeing a diminishing with temperature from 300 and 330 K. Table 3 shows how the values of E_{curve} are similar for h-V SM and n-V SM bilayers, in the range from 300 to 310 K. Both SM showed the same behavior against temperature, where an increase in temperature is

Table 4
Bending modulus (k^b), spontaneous mean curvature C_0, first moment, P^1, Gaussian modulus (k_G^b) and bending energy (E_{curve}) of binary bilayers composed of SM and Cer 310K.

SM:Cer (molar ratio)	1:0	3:1	1:1	1:3
		k^b/k_BT		
h-V SM:h-V Ce	30.2 ± 0.3	27.7 ± 0.9	35.2 ± 0.9	22.1 ± 0.7
h-V SM:n-V Cer	30.2 ± 0.3	31.9 ± 0.9	28.3 ± 0.8	30.4 ± 0.7
		C_0/nm		
h-V SM:h-V Cer	−1.06 ± 0.18	−0.83 ± 0.12	−0.632 ± 0.09	−0.94 ± 0.15
h-V SM:n-V Cer	−1.06 ± 0.18	−0.65 ± 0.16	−0.58 ± 0.09	−0.483 ± 0.06
		$P^1/(k_BT)$		
h-V SM:h-V Cer	−16.0 ± 0.6	−11.5 ± 1.1	−11.1 ± 0.9	−10.4 ± 1.7
h-V SM:n-V Cer	−16.0 ± 0.6	−10.4 ± 1.3	−8.18 ± 0.7	−7.34 ± 0.8
		$k_G^b/(k_BT)$		
h-V SM:h-V Cer	87 ± 7	75 ± 6	71 ± 8	66 ± 7
h-V SM:n-V Cer	87 ± 7	65 ± 9	47 ± 5	37 ± 3
		$E_{curve}/(k_BT)$		
h-V SM:h-V Cer	1858 ± 220	1637 ± 143	1785 ± 130	1381 ± 168
h-V SM:n-V Cer	1858 ± 220	1618 ± 100	1298 ± 125	1224 ± 103

reflected in a diminution in E_{curve}. This result agrees with the fact that the energy required to convert a bilayer with a planar shape into a spherical conformation diminishes with the rigidity of the lipid bilayer. Thus, E_{curve} diminished a 10% between 310 and 330 K for h-V SM, while a descent of 14% was measured for n-V SM. These differences reflect the contribution of the hydroxyl group in h-V SM to form hydrogen bonds between neighboring molecules.

3.2. Mechanical properties of binary mixtures of SM and Cer

To explore the impact of the transformation of SM into h-V Cer and n-V Cer, binary SM/Cer bilayers have been studied as a simplified model of a sperm membrane after its activation by the enzyme sphingomyelinase. Thus, h-V SM was considered as the common sphingomyelin in all the cases, and different ratios of h-V Cer or n-V Cer were considered in our study (Table 4). The binary bilayers containing n-V Cer reached a maximum value of k^b at 25% in n-V Cer which decreased at a 1:1 molar ratio. For h-V Cer, they reached a maximum value of k^b at 50%, diminishing at 75%. When binary bilayers contained 75% Cer, k^b increased in the presence of n-V Cer, showing a tendency to form more rigid bilayers. These results contrast with the ones shown by h-V Cer in which a diminishing was estimated. Interestingly, binary bilayers containing 75% h-V Cer were the most flexible, as they correspond to the lowest k^b value, showing values even below to the corresponding ones of pure h-V SM bilayers.

Regarding the Gaussian curvature modulus, the presence of h-V Cer induced the h-V SM bilayer toward lower values of K_G^b, being this behavior more noticeable in presence of n-V Cer (Table 4).

Fig. 6 shows a diminishing in the values of E_{curve} in presence of Cer. This behavior is much more noticeable in presence of n-V Cer than in presence of h-V Cer. This trend is an evidence of the increase in the bilayer instability with the ceramide composition, specially in presence of n-V Cer. This behavior can be associated, in a first instance, with the biological mechanism that take place during the fertilization process, which involves the acrosomal reaction. This briefly consists in the fusion of the outer leaflet of the acrosomal membrane and the inner leaflet of the plasma membrane of the sperm, forming discontinuities on its head, allowing the release of the acrosomal content.

Basically, this mechanism matches perfectly with the Energy of Curvature depicted in Fig. 6, where a diminishing in E_{curve} is estimated in presence of ceramides, that can be associated with the preliminary stages of the acrosomal reaction.

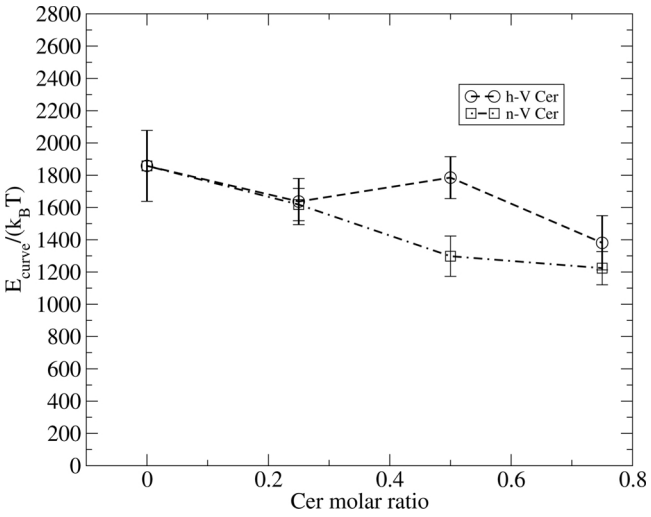

Fig. 6. E_{curve} as a function of the molar ratio of ceramide and sphingomyelin (h-V SM) in different binary bilayers.

4. Concluding remarks

This study presents valuable information about the mechanical properties of bilayers of SM and Cer molecules with VLCPUFA that are present in the cell membrane of spermatozoa of some mammals, especially in rats and mice (the laboratory rodents most widely used in biomedical studies). We have chosen a pair of SM that can be found in the head of rat spermatozoa, and a pair of Cer that are generated at expenses of such SM after completion, in vitro, of the acrosomal reaction. The SM and Cer species chosen for this study contained a non-hydroxy (n-V) or 2-hydroxy (h-V) very long chain polyunsaturated fatty acid with 30 carbon atoms (30:5).

Computer simulations provided insight with atomic detail into the mechanical properties of SM and Cer bilayers with VLCPUFA. Thus, h-V and n-V SM showed almost the same behavior in comparison with h-V Cer and n-V Cer that showed a completely different behavior of each other, and even with both SM.

This different behavior between SM and Cer was extended to other properties such as lateral pressure profile $\pi(z)$, compressibility modulus K_A, bending modulus k^b, spontaneous curvature C_0, gaussian curvature modulus k_G^b, and energy of curvature E_{curve}. In line with these properties, it was evidenced how the n-V Cer content is a crucial parameter for the stability of the bilayers formed.

Regions with high concentrations in ceramides can be formed in biological membranes by enzymatic catalysis of SM by sphingomyelinase. In the present study, when Cer was added to a fluid h-V SM bilayer, the mechanical stability of the binary SM/Cer bilayers resulted dramatically affected, as it is deduced from its curvature energy (E_{curve}).

Thus, the variation in E_{curve} can be associated with the change in the membrane mechanical properties of the spermatozoa head during the acrosomal reaction that permit the fusion of both sperm membranes, the discontinuities of the head sperm membrane, and the release of the acrosomal content.

In summary, we conclude that the variation of the curve energy of the spermatozoa membrane due to the sphingomyelinase reaction, may be a critical property during the preliminary steps of the fecundation process.

Acknowledgments

H.A.G. acknowledges Universidad del Bio-Bio for their financial support through the project DIUBB 153109 2/R(2015-2016) and to the program Becas iberoamericas- Jovenes profesores e investigadores for the support given through the Santander Universidades program. This research was partially supported by grants from Universidad Nacional de San Luis and ANPCyT-Argentina.

References

Bahamonde-Padilla, V.A., Espinoza, J., Weiss-Lopez, B.E., Lopez Cascales, J.J., Montecinos, R., Araya-Maturana, R., 2013. Effect of lithium on the properties of a liquid crystal formed by sodium dodecylsulphate and decanol in aqueous solution. J. Chem. Phys. 139, 14703–14711.

Barenholz, Y., Thompson, T.E., 1980. Sphingomyelins in bilayers and biological membranes. Biochim. Biophys. Acta 604 (2), 129–158.

Berendsen, H.J.C., Postma, J.P.M., van Gunsteren, W.F., Hermans, J., 1981. Intermolecular Forces. D. Reidel Publishing Company.

Berendsen, H.J.C., Postma, J.P.M., van Gunsteren, W.F., DiNola, A., Haak, J.R., 1984. Molecular dynamics with coupling to an external bath. J. Chem. Phys. 81 (8), 3684–3690.

Berendsen, H.J.C., Van der Spoel, D., Vandrunen, R.R., 1995. GROMACS a message-passing parallel molecular-dynamics implementation. Comput. Phys. Commun. 91 (1-3), 43–56.

Chiu, S.W., Vasudevan, S., Jakobsson, E., Mashl, R.J., Scott, H.L., 2003. Structure of sphingomyelin bilayers: a simulation study. Biophys. J. 85 (6), 3624–3635.

Claessens, M.M.A.E., van Oort, B.F., Leermakers, F.A.M., Hoekstra, F.A., Cohen Stuart, M.A., 2004. Charged lipid vesicles: Effect of salts on bending rigity, stability ans size. Biophysical J. 87, 3882–3893.

Darden, T., York, D., Pedersen, L., 1993. Particle mesh Ewald, an N.log(N) method for Ewald sums in large systems. J. Chem. Phys. 98 (12), 10089–10092.

der Laan van den Brink-van, J.A. Killian, and B. de Kruijff Nonbilayer lipids affect peripheral and integral membrane proteins via changes in the lateral pressure profile. Biochim.Biophys.Acta 1666(1-2)(2004)275-288.

Doktorova, M., Harries, D., Khelashvili, G., 2017. Determination of bending rigidity and tilt modulus of lipid membranes from real-space fluctuation analysis of molecular dynamics simulations. Phys. Chem. Chem. Phys. 19, 16806–16818.

Dutagaci, B., Becker-Baldus, J., Faraldo-Gomez, J.D., Glaubitz, C., 2014. Ceramide-lipid interactions studied by md simulations and solid-state nmr. BBA-Biomembranes 1838, 2511–2519.

Egberts, E., Marrink, S.J., Berendsen, H.J.C., 1994. Molecular dynamics simulation of a phospholipid membrane. Eur. Biophys. J. 22 (6), 423–436.

Essmann, U., Perera, L., Berkowitz, M.L., Darden, T., Lee, H., Pedersen, L.G., 1995. A smooth particle mesh Ewald method. J. Chem. Phys. 103 (19), 8577–8593.

Furland, N.E., Oresti, G.M., Antollini, S.S., Venturino, A., Maldonado, E.N., Aveldaño, M.I., 2007. Very long-chain polyunsaturated fatty acids are the major acyl groups of sphingomyelins and ceramides in the head of mammalian spermatozoa. J. Biol. Chem. 282 (25), 18151–18161.

Giner Casares, J.J., Camacho, L., Martín Romero, M.T., López Cascales, J.J., 2010. Methylene blue adsorption on a dmpa lipid langmuir monolayer. ChemPhysChem 11 (10), 2241–2247.

Goetz, R., Gompper, G., Lipowsky, R., 1999. Mobility and elasticity of self-assembled membranes. Phys. Rev. Letters 82 (1), 221–224.

Guo, S., Moore, T.C., Iacovella, C.R., Strickland, L.A., McCabe, C., 2013. Simulation study of the structure and phase behavior of ceramide bilayers and the role of lipid head-group chemistry. J. Chem. Theory Comput. 9, 5116–5126.

W. Helfrich and H. Rennschub Landau theory of the lamellar to cubic phase transition. J. Phys. Colloques (51):c7-189-C7-195, 1990.

B. Hess, H. Bekker, H.J.C. Berendsen, and H.J.C. Fraaije LINCS: a linear constraint solver for molecular simulations. J. Comp. Chem. (18) (1997) 1463-1472.

Hu, M., de Jong, D.H., Marrink, S.J., Desermo, M., 2013. Gaussian curvature elasticity determined from global shape transformations and local stress distributions: a comparative study using the martini model. Faraday Discuss. 161, 365–382.

HyperChem Package developed by and licensed from HyperCube, Inc., 1992.

Hyvonen, M.T., Kovanen, P.T., 2003. Molecular dynamics simulation of sphingomyelin bilayer. J. Phys. Chem. B 107, 9102–9108.

Jimenez-Rojo, N., Garcia-Arribas, A.B., Sot, J., Alonso, A., Goñi, F.M., 2014. Lipid bilayers containing sphingomyelins and ceramides of varying n-acyl lengths: A glimpse into sphingolipid complexity. BBA-Biomembranes 1838, 456–464.

López Cascales, J.J., Huertas, M.L., de la Torre, J.G., 1997. Molecular dynamics simulation of a dye molecule in the interior of a bilayer: 1,6-diphenyl-1,3,5-hexatriene in dipalmitoylphosphatidylcholine. Biophys. J. 69 (1), 1–8.

López Cascales, J.J., Cifre, J.G.H., de la Torre, J.G., 1998. Anaesthetic mechanism on a model biological membrane: a molecular dynamics simulation study. J. Phys. Chem. B 102 (3), 625–631.

López Cascales, J.J., Otero, T.F., Smith, B.D., Gonzalez, C., Marquez, M., 2006. Model of an asymmetric DPPC/DPPS membrane: effect of asymmetry on the lipid properties. A molecular dynamics simulation study. J. Phys. Chem. B 110 (5), 2358–2363.

López Cascales, J.J., Oliveira Costa, S.D., Garro, A., Enriz, R.D., 2012. Mechanical properties of binary DPPC/DPPS bilayers. RSC Advances 2, 11743–11750.

Levine, Z.A., Venable, R.M., Watson, M.C., Lerner, M.G., Shea, J.E., Pastor, R.W., Brown, F.L.H., 2014. Determination of biomembrane bending moduli in fully atomistic simulations. J. Am. Chem. Soc. 136, 13582–13585.

Li, X.M., Smaby, J.M., Momsen, M.M., Brockman, H.L., Brown, R.E., 2000. Sphingomyelin interfacial behavior: the impact of changing acyl chain composition. Biophys. J. 78 (4), 1921–1931.

Lindahl, E., Edholm, O., 2000. Spatial and energetic-entropic decomposition of surface tension in lipid bilayers from molecular dynamics simulations. J. Chem. Phys. 113 (9), 3882–3893.

E. Lindahl, B Hess, and D. van der Spoel Gromacs 3.0: a package for molecular simulation and trajectory analysis. J. Mol. Modeling 7(8)(2001)306-317.

Maulik, P.R., Sripada, P.K., Shipley, G.G., 1991. Structure and thermotropic properties of hydrated n-stearoyl sphingomyelin bilayer membranes. Biochim.Biophys.Acta 1062 (2), 211–219.

Mombelli, E., Morris, R., Taylor, W., Fraternali, F., 2003. Hydrogen-bonding propensities of sphingomyelin in solution and in a bilayer assembly: a molecular dynamics study. Biophys. J. 84 (3), 1507–1517.

Needham, D., Nunn, R.S., 1990. Elastic deformation and failure of lipid bilayer membranes containing cholesterol. Biophys. J. 58 (4), 997–1009.

Niemela, P., Hyvonen, M.T., Vattulainen, I., 2004. Structure and dynamics of sphingomyelin bilayer: insight gained through systematic comparison to phosphatidylcholine. Biophys. J. 87 (5), 2976–2989.

Niemela, P.S., Hyvonen, M.T., Vattulainen, I., 2006. Influence of chain length and unsaturation on sphingomyelin bilayers. Biophys. J. 90 (3), 851–863.

Oresti, G.M., Reyes, J.G., Luquez, J.M., Osses, N., Furland, N.E., Aveldaño, M.I., 2010. Differentiation-related changes in lipid classes with long-chain and very long-chain polyenoic fatty acids in rat spermatogenic cells. J. Lipid Res. 51 (10), 2909–2921.

G.M.Oresti, J.M. Luquez, N.E. Furland, and M.I Aveldaño Uneven distribution of ceramides, sphingomyelins and glycerophospholipids between heads and tails of rat spermatozoa. Lipids 46(12)(2011)1081-1090.

Oresti, G.M., Peñalva, D.A., Luquez, J.M., Antollini, S.S., Aveldaño, M.I., 2015. Lipid biochemical and biophysical changes in rat spermatozoa during isolation and functional activation in vitro. Biol. Reprod. 93 (6), 140.

Orsi, M., Haubertin, D.Y., Sanderson, W.E., Essex, J.W., 2008. A quantitative coarse-grain model for lipid bilayers. J. Chem. Phys. B. 112, 802–815.

Pan, J., Tristram-Nagle, S., Kucerka, N., Nagle, J.F., 2008. Temperature dependence of structure, bending rigidity and bilayer interactions of dioleoylphosphatidylcholine bilayers. Biophysical J. 94, 117–124.

S.A. Pandit and H.L. Scott Molecular-dynamics simulation of a ceramide bilayer. J.Chem. Phys. 124(1) (2006) 14708.

Peñalva, D.A., Furland, N.E., López, G.H., Aveldaño, M.I., Antollini, S.S., 2013. Unique thermal behavior of sphingomyelin species with nonhydroxy and 2-hydroxy very-long-chain (c28-c32) pufas. J. Lipid Res. 54, 2225–2235.

D.A. Peñalva, G.M. Oresti, F. Dupuy, S.S. Antollini, B. Maggio, M.I Aveldaño, and M.L. Fanani Atypical surface behavior of ceramides with nonhydroxy and 2-hydroxy very long-chain (c28-c32) pufas. Biochim. Biophys. Acta 1838(3)(2014)731-738.

Peñalva, D.A., Wilke, N., Maggio, B., Aveldaño, M.I., Fanani, M.L., 2014b. Surface behavior of sphingomyelins with very long chain polyunsaturated fatty acids and effects of their conversion to ceramides. Langmuir 30 (15), 4385–4395.

Piotto, S., Trapani, A., Bianchino, E., Ibarguren, M., Lopez, D.J., Busquets, X., Concilio, S., 2014. The effect of hydroxylated fatty acid-containing phospholipids in the remodeling of lipid membranes. BBA-Biomembranes 1838, 1509–1517.

J. A. Pople and G. A. Segal Approximate self-consistent molecular orbital theory.3. CNDO results for AB2 and AB3 systems. J. Chem. Phys. 44(9) (1966) 3289.

Porasso, R.D., Bennett, W.F.D., Oliveira-Costa, S.D., López Cascales, J.J., 2009. Study of the benzocaine transfer from aqueous solution to the interior of a biological membrane. J. Phys. Chem. B 113 (29), 9988–9994.

Poulos, A., Sharp, P., Johnson, D., White, I., Fellenberg, A., 1986. The occurrence of polyenoic fatty acids with greater than 22 carbon atoms in mammalian spermatozoa. Biochem. J. 240 (3), 891–895.

Poulos, A., Johnson, D.W., Beckman, K., White, I.G., Easton, C., 1987. Occurrence of unusual molecular species of sphingomyelin containing 28-34-carbon polyenoic fatty acids in ram spermatozoa. Biochem. J. 248 (3), 961–964.

Ramstedt, B., Slotte, J.P., 2002. Membrane properties of sphingomyelins. FEBS Lett. 531 (1), 33–37.

Rawicz, W., Olbrich, K.C., McIntosh, T., Needham, D., Evans, E., 2000. Effect of chain length and unsaturation on elasticity of lipid bilayers. Biophys. J 79 (1), 328–339.

Robinson, B.S., Johnson, D.W., Poulos, A., 1992. Novel molecular species of sphingomyelin containing 2-hydroxylated polyenoic very-long-chain fatty acids in mammalian testes and spermatozoa. J. Biol. Chem. 267 (3), 1746–1751.

Ryckaert, J.P., Bellemans, A., 1978. Faraday Discuss. Chem. Soc. 66, 95.

Safran, S.A., 1999. Curvature elasticity of thin films. Adv. Phys. 48 (4), 395–448.

Shearman, G.C., Ces, O., Templer, R.H., Seddon, J.M., 2006. Inverse lyotropic phases of lipids and membranes. J. Phys.: Condensed Matter 18, 1105–1124.

Slotte, J.P., Ramstedt, B., 2007. The functional role of sphingomyelin in cell membranes. Eur. J. Lipid Sci. Tech. 109, 977–981.
Templer, R.H., Castle, S.J., Curran, A.R., Rumbles, G., Klug, D.R., 1998. Sensing isothermal changes in the lateral pressure in model membranes using di-pyrenyl phosphatidylcholine. Faraday Discuss. 111 (111), 41–53.
Trauble, H., Haynes, D.H., 1971. The volume change in lipid bilayer lamellae at the crystalline-liquid crystalline phase transition. Chem. Phys. Lipids 7 (4), 324–335.
Valtierra, F.X.S., Mateos, M.V., Aveldaño, M.I., Oresti, G.M., 2017. Sphingomyelins and ceramides with very-long-chain pufa are excluded from low-density, raft-like domains in differentiating spermatogenic cells. J.Lipid Res. 58 (3), 529–542.
W.F. van Gunsteren and H.J.C. Berendsen Biomos, nijenborgh 4, 9747 ag groningen, the netherlands. Groningen molecular simulation (GROMOS) library manual. 1987.
Veiga, M.P., Arrondo, J.L.R., Goñi, F.M., Alonso, A., 1999. Ceramides in phospholipid membranes: Effects on bilayer stability and transition to nonlamellar phases. Biophys. J. 76, 342–350.
Venable, R.M., Brown, F.-L.H., Pastor, R.W., 2015. Mechanical properties of lipid bilayers from molecular dynamics simulation. Chem. Phys. Lip. 192, 60–74.
Watson, M.C., Morriss-Andrews, A., Welch, P.M., Brown, F.L.H., 2013. Thermal fluctuations in shape, thickness and molecular orientation in lipid bilayers.ii. finite surface tensions. J. Chem. Phys. 139, 84706–84718.
S.R. Zanetti, M.M. de Los Angeles, D.E. Rensetti, M.W. Fornes, and M.I. Aveldaño Ceramides with 2-hydroxylated, very long-chain polyenoic fatty acids in rodents: From testis to fertilization-competent spermatozoa. Biochimie 92(12)(2010)1778-1786.